Downloaded via UNIV OF VIRGINIA on November 1, 2018 at 16:42:28 (UTC). See https://pubs.acs.org/sharingguidelines for options on how to legitimately share published articles.

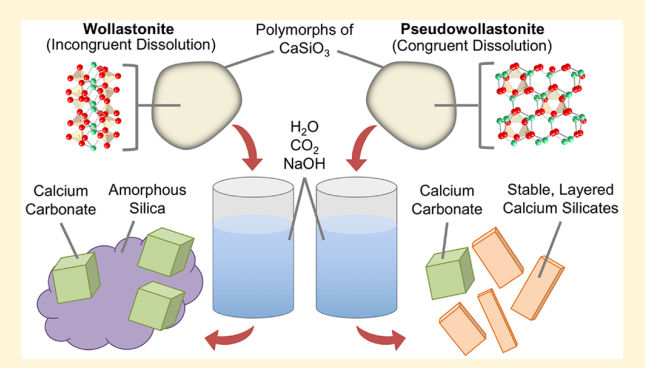
Cite This: Environ. Sci. Technol. Lett. 2018, 5, 558–563

# Calcium Silicate Crystal Structure Impacts Reactivity with CO<sub>2</sub> and **Precipitate Chemistry**

Dan A. Plattenberger, † Florence T. Ling, † Zhiyuan Tao, † Catherine A. Peters, † and Andres F. Clarens\*,†

<sup>†</sup>Civil and Environmental Engineering, University of Virginia, Charlottesville, Virginia 22904, United States

ABSTRACT: The reaction of  $\mathrm{CO}_{2(\mathrm{aq})}$  with calcium silicates creates precipitates that can impact fluid flow in subsurface applications such as geologic CO2 storage and geothermal energy. These reactions nominally produce calcium carbonate (CaCO<sub>3</sub>) and amorphous silica (SiO<sub>x</sub>). Here we report evidence that the crystal structure of the parent silicate determines the way in which it reacts with CO2 and the resulting structures of the reaction products. Batch experiments were performed using two polymorphs of a model calcium silicate (CaSiO<sub>3</sub>), wollastonite (chain-structured) and pseudowollastonite (ring-structured), at elevated temperatures (150 °C) and partial pressures of CO<sub>2</sub> (0-11 MPa). Reaction of CO<sub>2(aq)</sub> with wollastonite produced CaCO<sub>3</sub> and SiO<sub>x</sub>,



whereas reaction of CO<sub>2(aq)</sub> with pseudowollastonite produced platelike crystalline calcium silicate phases, along with CaCO<sub>3</sub> and SiO<sub>x</sub>. A reaction mechanism that explains the observations in relation to dissolution of the parent silicate, the pH of the solution, and the presence of nucleation sites is proposed. The mechanism is supported with inductively coupled plasma optical emission spectrometry measurements and scanning electron microscopy/transmission electron microscopy-selected-area electron diffraction characterization of solid products. These findings are important for a number of reasons, among them, the fact that the crystalline silicate precipitates are more stable than CaCO3 under low-pH conditions, which could be valuable for creating permanent seals in subsurface applications.

# INTRODUCTION

In deep subsurface environments such as those associated with hydraulic fracturing, CO2 storage, and enhanced geothermal energy production, there is growing interest in managing environmental impacts associated with undesirable fluid migration. 1-6 The targeted deployment of mineral precipitation reactions is one strategy that has been proposed to manage the fate of fluid flow properties in porous media.<sup>7</sup> Calcium silicates make up a common and broad class of minerals that can be used in these applications. They dissolve in acid to produce cations (Ca<sup>2+</sup>) and amorphous silica (SiO<sub>2</sub>), which can create an opportunity for pore plugging.

$$CaSiO_{3(s)} + 2H^{+} \leftrightharpoons Ca^{2+} + SiO_{2(am)} + H_{2}O$$
 (1)

The rates at which the cation and silica are released into solution have been shown to vary considerably on the basis of the crystal structure of the parent compound, even among minerals having the same chemical formula. 10,111 Wollastonite, CaSiO<sub>3</sub>, dissolves incongruently, resulting in nonstoichiometric release of calcium and silicon. 12,13 Wollastonite has a pyroxenoid silicate chain structure and resists rapid Si leaching due to the strength of Si-O bonds in the silicate chains, resulting in preferential Ca leaching. In contrast, the polymorph pseudowollastonite has an isolated trisilicate ring

structure in which the Ca2+ ions are weakly bonded to O atoms resulting in rapid, stoichiometric dissolution and equal release of Ca and Si during dissolution. 14,15

Under conditions where  $CO_{2(aq)}$  is present, the cation can form a complex with carbonate ions and precipitate as calcium carbonate (CaCO<sub>3</sub>).

$$Ca^{2+} + CO_{2(aq)} + H_2O \Rightarrow CaCO_{3(s)} + 2H^+$$
 (2)

In this reaction, CO<sub>2</sub> provides both the reactant (carbonate ions) and the source of hydrogen ions (carbonic acid). If CO<sub>2</sub> is present in sufficiently high concentrations, it will drive the reaction to the left. Understanding these competing effects is critical for controlling this chemistry in engineered applica-

When wollastonite dissolves in the presence of CO<sub>2(ag)</sub>, a calcium-depleted leached layer forms and the calcium ions can react with  $CO_{2(aq)}$  to form solid carbonates  $^{16}$  in accordance with eqs 1 and 2. In contrast, we hypothesized that when pseudowollastonite dissolves in the presence of  $CO_{2(aq)}$ , the

Received: July 26, 2018 August 21, 2018 Accepted: August 24, 2018 Published: August 24, 2018

<sup>&</sup>lt;sup>‡</sup>Civil and Environmental Engineering, Princeton University, Princeton, New Jersey 08544, United States

Table 1. Selection of Experimental Conditions and Reaction Products Described in This Work<sup>a</sup>

	pCO <sub>2</sub> (MPa)	[NaOH] (M)	pH <sup>b</sup>	interface	wollastonite reaction products	pseudowollastonite reaction products	analytical techniques
0	0	0.1	10.5	sand	Ir	Ir	SEM, EDS
1	1.1	0	3.9	sand	Ir > Ara > Cal	$Ir > Ara \gg PL$	SEM, EDS, XRD
2	1.1	0.1 (NaCl)	3.9	sand	Ir > Cal ≫ Ara	$Ir > Ara \gg PL$	SEM, EDS, XRD
3	1.1	0.1	6.7	none	Ir > Cal ≫ Ara	Ir > Ara	SEM, EDS, XRD
4 <sup>c</sup>	1.1	0.1	6.7	sand	Ir > Cal ≫ Ara	PL > Ara > Ir	SEM, EDS, XRD
5	1.1	0.1	6.7	sand	Ir > Cal ≫ Ara	PL > Ara > Ir	SEM, EDS, XRD, TEM
6	5.5	0.1	5.9	sand	Ir > Cal	Cal > Ir	SEM, EDS
7	11	0.1	5.7	sand	Ir > Cal	Cal > Ir	SEM, EDS

<sup>a</sup>Products listed in order of prevalence, as determined by SEM-EDS analysis coupled with XRD. Here, "irregular" phases (IR) include amorphous silica as well as unreacted CaSiO3, solid carbonates include calcite (Cal) and aragonite (Ara), and layered calcium silicate phases [platelike (PL)] are also observed. <sup>b</sup>Calculated for batch solution at equilibrium with CO<sub>2</sub> at 150 °C using PHREEQC. <sup>c</sup>Experiment conducted at a low total pressure (1.1 MPa).

availability of cations and high concentrations of dissolved silica can result in precipitation of non-carbonate mineral phases with low ratios of cation to silica ( $\leq 1$ ) similar to tobermorite<sup>17</sup> [Ca<sub>5</sub>Si<sub>6</sub>O<sub>16</sub>(OH<sub>2</sub>)·4H<sub>2</sub>O] and magadiite<sup>18</sup> [Na-Si<sub>2</sub>O<sub>13</sub>(OH)<sub>3</sub>·4H<sub>2</sub>O]. Those products have been noted for their high strengths, 19 adsorption properties, 20 and low reactivities,<sup>21</sup> and the availability of nucleation sites has been shown to play an important role in controlling the morphology and rate of their precipitation. 22,23

The reaction of calcium silicates with CO2 has been well studied in the context of carbon sequestration. Examples include reactions in basalts 24,25 and exposed mantle peridotites,<sup>26</sup> engineered weathering of silicate minerals,<sup>27,2</sup> and sequestration in deep saline aquifers.<sup>29</sup> We are interested in these reactions not because of their potential to mineralize CO2 directly but because of their potential to create precipitates other than carbonates. Silicates could be delivered into pore spaces, where resulting precipitates could seal porous and fractured rocks and cements or stabilize and encase  $carbonate\ precipitates.^{30}$ 

Here we present new evidence of the role of crystal structure (rather than simply elemental composition) of the parent silicate in controlling the chemistry of the precipitated minerals. This is a connection that has not yet been reported in the literature and is one that could have important implications in a number of subsurface applications requiring strength and stability. Batch experiments were performed using wollastonite and pseudowollastonite under a range of pH, pressure, and CO2 conditions to establish a proposed mechanistic understanding of the dissolution and precipitation reactions that control the formation of these chemically stable mineral phases.

#### MATERIALS AND METHODS

Materials. A citrate-nitrate gel autocombustion method was used to make a calcium silicate ash that was calcined at 950 or 1250  $^{\circ}\text{C}$  for 2 h to produce wollastonite or pseudowollastonite, respectively. The calcium silicate powders were then ground separately and sieved to isolate the 74-149  $\mu$ m fraction. The crystal structures and morphologies of the calcium silicates were confirmed via powder X-ray diffraction (XRD), coupled with scanning electron microscopy (SEM) and energy dispersive X-ray spectroscopy (EDS). In experiments in which sand was used to test the effects of heterogeneous nucleation, Ottawa sand (US Silica, F-50) was sieved to obtain the 250–595  $\mu$ m fraction, washed in 1 N HCl (Sigma-Aldrich), and rinsed with deionized water (>18.0 M $\Omega$ 

cm). Sodium hydroxide (98% NaOH, Sigma-Aldrich) and sodium chloride (99% NaCl, EM Science) were used as received.

Batch Experiments. To investigate these reactions, experiments were conducted in batch systems to isolate the chemical processes and enable observation of reaction products, while limiting macro-scale mass-transfer limitations and heterogeneity that exists in column experiments. For each set of experimental conditions, 15 mg each of wollastonite and pseudowollastonite powder were placed into separate, identical, Teflon boats (approximately 0.75 cm<sup>3</sup>) and placed in a single Teflon-lined stainless-steel pressure vessel. Within each boat, 1 g of sand and 0.5 mL of deionized water (with various concentrations of NaOH and/or NaCl) were added. Pressure vessels were heated to 150 ± 3 °C. CO<sub>2</sub> was injected into the vessels via a syringe pump (Teledyne ISCO), and the concentration of dissolved CO2 was calculated by its partial pressure in the headspace using PHREEQC, equilibrated with the water phase, for each CO<sub>2</sub> concentration that was tested. Once the CO<sub>2</sub> pressure equilibrated, the pump was switched to nitrogen gas and the pressure was increased to 15.5 MPa. Each experiment was conducted for 24 h, and afterward, the samples, in the Teflon boats, were oven-dried at 75 °C where sheet silicate precipitates are not expected to form. 32,33 Upon drying, the sand and powders became separable, and the powders were then rinsed three times to remove any remaining NaOH and dried at 50 °C for 12 h. The products of select samples were then divided, and a portion was acid-washed in a pH 5.5 acetic acid/sodium acetate-buffered solution for 6 h.<sup>34</sup> To remove the acid, those samples were again rinsed and oven-

**Analytical Methods.** The reaction products were analyzed via SEM-EDS (FEG Environmental-SEM, Oxford AZtec EDS system) for morphology and elemental composition and via powder XRD (Bruker D8 Advance) for phase identification. Data were collected with a Ag tube source ( $\lambda = 0.56 \text{ Å}$ ) over a  $2\theta$  range of 4-20°, with a step size of 0.025-0.05°. Identification was performed using the powder diffraction database in Diffrac.Eva version 3.1 (Bruker). For single particles from one sample, transmission electron microscopy (TEM), selected-area electron diffraction (SAED), and additional EDS were conducted [FEI Talos (S)TEM, 200 kV]. Inductively coupled plasma optical emission spectrometry (ICP-OES, Thermo Scientific iCap 6200) was also used to analyze aqueous phases to determine relative dissolution rates of wollastonite and pseudowollastonite.

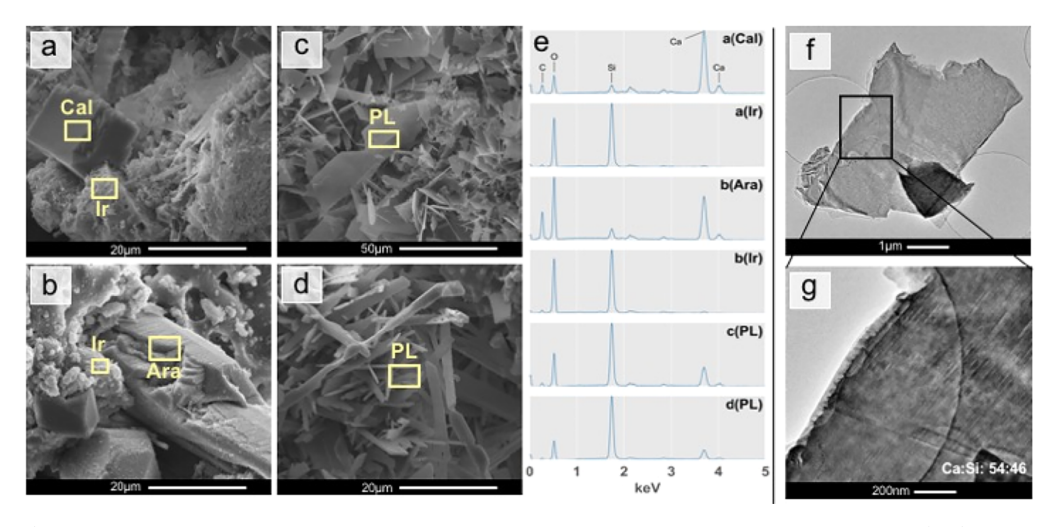


Figure 1. (a-d) Representative SEM micrographs of the phases produced in these experiments, including calcite (Cal), aragonite (Ara), and irregular silica phases (Ir). At elevated pH values and moderate dissolved carbonate concentrations, appreciable quantities of platelike (PL) calcium silicates are produced (c and d). (e) EDS spectra are presented for each of the identified phases in panels a-d. The spectra show that the PL phases are rich in both calcium and silica. (f and g) TEM micrographs show the nature of the PL phases, and EDS confirms an abundance of Si and Ca.

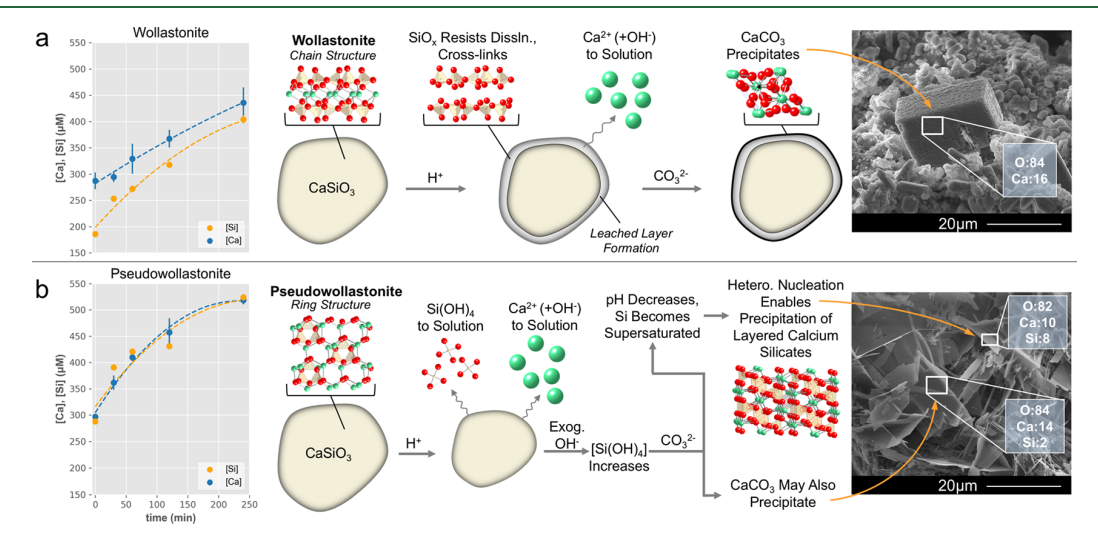


Figure 2. Proposed mechanism for how the crystal structures of (a) wollastonite and (b) pseudowollastonite, both polymorphs of  $CaSiO_3$ , influence the reactions that proceed in the presence of  $CO_{2(aq)}$ . Wollastonite dissolves nonstoichiometrically, as evidenced by ICP-OES measurements of dissolved Si and Ca. The resulting leached layer of  $SiO_x$  is depicted, as is the reaction of calcium with dissolved carbonate to generate  $CaCO_3$ . Pseudowollastonite dissolves congruently. The elevated concentration of dissolved silica promotes precipitation of layered calcium silicates. In parallel,  $CaCO_3$  may precipitate, consuming dissolved carbonate and some calcium ions.

## ■ RESULTS AND DISCUSSION

Layered Calcium Silicate Formation. The experiments conducted here, summarized in Table 1, yielded very different products for wollastonite and pseudowollastonite. When wollastonite reacted with  $\mathrm{CO}_{2(\mathrm{aq})}$ , only amorphous silica and  $\mathrm{CaCO}_3$  formed. Conversely, pseudowollastonite yielded a variety of morphologies observed via SEM, suggesting the presence of multiple mineral phases. For each experiment, the relative abundance of reaction products is listed in order of prevalence based on qualitative SEM–EDS coupled with XRD. For instances of  $\mathrm{CaCO}_3$ , calcite and aragonite were identified via XRD, except in samples 0, 6, and 7, where calcite was reported. Figure 1 presents representative micrographs and EDS spectra of the morphologies described in Table 1. The layered calcium silicate phases are likely crystalline calcium

silicate hydrates. TEM–SAED confirmed that the material was crystalline but did not match pseudowollastonite. TEM–EDS showed that one of the platelets had a 54:46 Ca:Si ratio. Previous work<sup>35</sup> identified trace amounts of nanoscale calcium silicate hydrates after reaction of wollastonite with CO<sub>2</sub>, while others<sup>36</sup> noted silicate polymerization during carbonation of natural wollastonite under high-relative humidity conditions. To the best of our knowledge, no work to date has reported the formation of such dissimilar reaction products from polymorphs of the same parent silicate.

The differences observed between the reaction products of wollastonite and pseudowollastonite were sensitive to both the presence of  $\mathrm{CO}_2$  and pH. In experiment 0, where no  $\mathrm{CO}_2$  was present, no layered calcium silicate phases were observed from reaction of either polymorph. At high  $\mathrm{CO}_2$  concentrations

(experiments 6 and 7), CaCO<sub>3</sub> was the predominant reaction product and significantly more CaCO<sub>3</sub> existed in pseudowollastonite than in wollastonite reaction samples.

When calcium silicates reacted with intermediate concentrations of CO2, the reaction products depended on several factors, including the initial CaSiO3 crystal structure, pH, and the availability of heterogeneous nucleation sites (i.e., sand). Comparison of the results from experiments 3 and 5 suggests that, in pseudowollastonite experiments, nucleation sites are needed to yield layered calcium silicate precipitates. Also, when the pH was increased using 0.1 M NaOH (experiments 4 and 5), an abundance of platelike phases was observed. To better understand the role of Na in this reaction mechanism (because NaOH was used), experiment 2 was conducted at the same Na molar concentration as experiment 5, with NaCl rather than NaOH. Only a very small quantity of platelike phases was found in experiment 2, and the results nearly mirror those of experiment 1. In addition, XRD analyses suggest that calcite was the predominant CaCO<sub>3</sub> mineral in wollastonite samples and aragonite was predominant in pseudowollastonite samples. Because pseudowollastonite dissolves more rapidly, this observation is likely due to the relative concentrations of dissolved calcium in the aqueous phase.<sup>37</sup> All experiments were conducted at a high total pressure (15.5 MPa) to simulate conditions in the deep subsurface except experiment 4, which was conducted at 1.1 MPa, to confirm that total pressure had little to no effect on products.

Mechanism for Layered Calcium Silicate Formation. These experiments provide insight into the mechanism that governs the formation of layered calcium silicates instead of CaCO<sub>3</sub>. A schematic of the proposed mechanism is presented in Figure 2. Figure 2a depicts the reaction of wollastonite in water, where the pyroxenoid silicate chains lead to nonstoichiometric dissolution of calcium ions and a silica network that hinders further dissolution of calcium. Previous work<sup>38-41</sup> demonstrated that in silicate-glass corrosion, this leached layer of silica gel restructures and cross-links, effectively closing pores around the periphery of the glass. However, hydrolysis of Si-O bonds allows the limited release of polymerized vitreous silica, meaning the aqueous phase surrounding the solid surface is therefore calcium-rich but its silica concentration is relatively low, which is supported by the ICP-OES data in Figure 2a. When CO<sub>2</sub> is present, the precipitation of CaCO<sub>3</sub> is highly favorable. In contrast, Figure 2b depicts the case of pseudowollastonite reacting with water and CO<sub>2</sub>. The trisilicate rings are readily dissolved, releasing stoichiometric quantities of Ca and Si [silicic acid, Si(OH)<sub>4</sub>]. With the exogenous elevation of the pH (NaOH), the concentration of dissolved Si increases and becomes supersaturated, and Si forms complexes with calcium (and, possibly, carbon) and precipitates as layered calcium silicates, with the Ca:Si stoichiometry being dependent on the local ion concentrations. Simultaneously, some Ca may be consumed by the precipitation of CaCO<sub>3</sub>. Not depicted in the figure is the impact of temperature on the morphologies and crystal structures of precipitates, but previous work<sup>32,33</sup> and our experiments suggest that the layered calcium silicates are more prevalent at >120 °C. Experiments performed over longer time scales, not shown, produced similar results, suggesting the results are not time-dependent over the time scales evaluated

ICP-OES analyses confirmed that dissolution rates in CaSiO<sub>3</sub> could be driving the difference in precipitate

chemistry. Experiments were performed under conditions that mimicked the conditions of experiment 4 except HCl was used in place of  $\mathrm{CO}_2$  to prevent rapid  $\mathrm{CaCO}_3$  precipitation. The molar concentrations of aqueous  $\mathrm{Ca}$  and  $\mathrm{Si}$  (0.55 g of 74–150  $\mu\mathrm{m}$  CaSiO<sub>3</sub> in 500 mL of stirred water) upon reaching 150 °C are shown. The plots show that Ca dissolves more quickly than  $\mathrm{Si}$  in wollastonite but stoichiometrically in pseudowollastonite. Additionally, these experiments produced no crystalline silicate phases or  $\mathrm{CaCO}_3$  (as determined by SEM–EDS), which underscores the importance of  $\mathrm{CO}_2$  in the system.

The results of the acetic acid washing provide insights into the chemical stability of the layered calcium silicates produced relative to CaCO<sub>3</sub>. Representative SEM micrographs and layered EDS maps (Ca, Si, and C) of (a) unreacted pseudowollastonite, (b) products from CO<sub>2</sub>-reacted pseudowollastonite (experiment 4), and (c) products from CO<sub>2</sub>-reacted and acid-washed pseudowollastonite (experiment 4) are presented in Figure 3. The EDS maps in panel b show

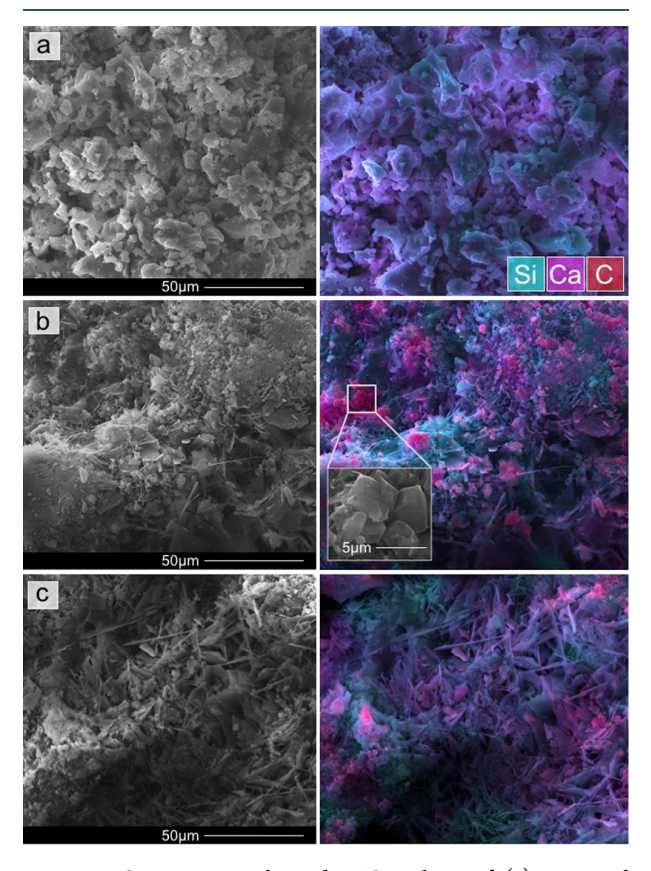


**Figure 3.** SEM micrographs and EDS analyses of (a) unreacted pseudowollastonite showed no evidence of CaCO<sub>3</sub>, while those from (b) reacted pseudowollastonite showed a significant quantity. (c) After acid washing, CaCO<sub>3</sub> was not observed while platelike phases remained unaltered.

intense regions of calcium and carbon that align with the regions that appear to be  $CaCO_3$ . The remainder (and majority) of the sample is comprised primarily of platelike phases, which remained entirely intact after acid washing, along with some irregular phases.  $CaCO_3$  could not be found in the acid-washed samples.

The chemical resilience of the layered crystalline calcium silicates suggests they could have important applications in subsurface engineering contexts, among others. While pseudowollastonite is less common than wollastonite in the environment, the role of ion concentration revealed here could be leveraged to deliver mixtures of other more abundant minerals that would produce ideal reactant concentrations to generate layered calcium silicates in applications such as geologic CO2 storage, geothermal energy, or hazardous waste containment. Pseudowollastonite nanoparticles or some combination of calcium and silica from waste streams delivered at the right ratios could create the pore conditions that would result in the precipitation of stable mineral phases, which could enable dramatic decreases in permeability, even in harsh environmental conditions. In ex situ carbon storage and cement applications, these results could inform novel ways to produce unreactive passivating layers on carbonates that would resist weathering and improve the long-term stability of the materials produced.

#### AUTHOR INFORMATION

## **Corresponding Author**

\*E-mail: andres@virginia.edu.

#### ORCID ®

Dan A. Plattenberger: 0000-0002-0775-2745 Catherine A. Peters: 0000-0003-2418-795X Andres F. Clarens: 0000-0002-0606-9717

Notes

The authors declare no competing financial interest.

# ■ ACKNOWLEDGMENTS

This work was supported by the U.S. Department of Energy National Energy Technology Laboratory (Grant DE-FE0026582) and the U.S. National Science Foundation (to A.F.C.) (CBET-1254839). The authors acknowledge the use of Princeton's Imaging and Analysis Center, which is partially supported by the Princeton Center for Complex Materials via the National Science Foundation-MRSEC program (DMR-1420541).

#### REFERENCES

- (1) Zhang, C.; Dehoff, K.; Hess, N.; Oostrom, M.; Wietsma, T. W.; Valocchi, A. J.; Fouke, B. W.; Werth, C. J. Pore-scale study of transverse mixing induced CaCO3 precipitation and permeability reduction in a model subsurface sedimentary system. *Environ. Sci. Technol.* **2010**, *44*, 7833–7838.
- (2) Nogues, J. P.; Fitts, J. P.; Celia, M. A.; Peters, C. A. Permeability evolution due to dissolution and precipitation of carbonates using reactive transport modeling in pore networks. *Water Resour. Res.* **2013**, *49*, 6006–6021.
- (3) Stack, A. G.; Fernandez-Martinez, A.; Allard, L. F.; Banuelos, J. L.; Rother, G.; Anovitz, L. M.; Cole, D. R.; Waychunas, G. A. Poresize-dependent calcium carbonate precipitation controlled by surface chemistry. *Environ. Sci. Technol.* **2014**, *48*, 6177–6183.
- (4) Poonoosamy, J.; Curti, E.; Kosakowski, G.; Grolimund, D.; Van Loon, L. R.; Mäder, U. Barite precipitation following celestite dissolution in a porous medium: A SEM/BSE and μ-XRD/XRF study. *Geochim. Cosmochim. Acta* **2016**, *182*, 131–144.
- (5) Hajirezaie, S.; Wu, X.; Peters, C. A. Scale formation in porous media and its impact on reservoir performance during water flooding. *J. Nat. Gas Sci. Eng.* **2017**, *39*, 188–202.
- (6) Li, Q.; Steefel, C. I.; Jun, Y. Incorporating nanoscale effects into a continuum-scale reactive transport model for CO2-deteriorated cement. *Environ. Sci. Technol.* **2017**, *51*, 10861–10871.

- (7) Tao, Z.; Fitts, J. P.; Clarens, A. F. Feasibility of carbonation reactions to control permeability in the deep subsurface. *Environ. Eng. Sci.* **2016**, 33, 778–790.
- (8) Deng, H.; Bielicki, J. M.; Oppenheimer, M.; Fitts, J. P.; Peters, C. A. Leakage risks of geologic CO2 storage and the impacts on the global energy system and climate change mitigation. *Clim. Change* **2017**, *144*, 151–163.
- (9) Zahasky, C.; Benson, S. M. Evaluation of hydraulic controls for leakage intervention in carbon storage reservoirs. *Int. J. Greenhouse Gas Control* **2016**, 47, 86–100.
- (10) Yang, Y.; Min, Y.; Jun, Y. Effects of al/si ordering on feldspar dissolution: Part II. the pH dependence of plagioclases' dissolution rates. *Geochim. Cosmochim. Acta* **2014**, *126*, 595–613.
- (11) Yang, Y.; Min, Y.; Lococo, J.; Jun, Y. Effects of al/si ordering on feldspar dissolution: Part I. crystallographic control on the stoichiometry of dissolution reaction. *Geochim. Cosmochim. Acta* **2014**, *126*, 574–594.
- (12) Casey, W. H.; Westrich, H. R.; Banfield, J. F.; Ferruzzi, G.; Arnold, G. W. Leaching and reconstruction at the surfaces of dissolving chain-silicate minerals. *Nature* **1993**, *366*, 253.
- (13) Schott, J.; Pokrovsky, O. S.; Spalla, O.; Devreux, F.; Gloter, A.; Mielczarski, J. A. Formation, growth and transformation of leached layers during silicate minerals dissolution: The example of wollastonite. *Geochim. Cosmochim. Acta* **2012**, *98*, 259–281.
- (14) Yang, H.; Prewitt, C. T. On the crystal structure of pseudowollastonite (CaSiO3). *Am. Mineral.* **1999**, 84, 929–932.
- (15) Casey, W. H. Glass and mineral corrosion: Dynamics and durability. *Nat. Mater.* **2008**, *7*, 930.
- (16) Bracco, J. N.; Grantham, M. C.; Stack, A. G. Calcite growth rates as a function of aqueous calcium-to-carbonate ratio, saturation index, and inhibitor concentration: Insight into the mechanism of reaction and poisoning by strontium. *Cryst. Growth Des.* **2012**, *12*, 3540–3548.
- (17) Galvánková, L.; MáSilko, J.; Solný, T.; Štěpánková, E. Tobermorite synthesis under hydrothermal conditions. *Procedia Eng.* **2016**, *151*, 100–107.
- (18) Fletcher, R. A.; Bibby, D. M. Synthesis of kenyaite and magadiite in the presence of various anions. *Clays Clay Miner.* **1987**, 35, 318–320.
- (19) Jackson, M. D.; Moon, J.; Gotti, E.; Taylor, R.; Chae, S. R.; Kunz, M.; Emwas, A.; Meral, C.; Guttmann, P.; Levitz, P.; Wenk, H.-R.; Monteiro, P. J. M. Material and elastic properties of al-tobermorite in ancient roman seawater concrete. *J. Am. Ceram. Soc.* **2013**, *96*, 2598–2606.
- (20) Mokhtar, M. Application of synthetic layered sodium silicate magadiite nanosheets for environmental remediation of methylene blue dye in water. *Materials* **2017**, *10*, 760.
- (21) Jackson, M. D.; Mulcahy, S. R.; Chen, H.; Li, Y.; Li, Q.; Cappelletti, P.; Wenk, H. Phillipsite and al-tobermorite mineral cements produced through low-temperature water-rock reactions in roman marine concrete. *Am. Mineral.* **2017**, *102*, 1435–1450.
- (22) Garrault-Gauffinet, S.; Nonat, A. Experimental investigation of calcium silicate hydrate (CSH) nucleation. *J. Cryst. Growth* **1999**, 200, 565–574.
- (23) Ma, Y.; Liu, N.; Jin, X.; Feng, T. Hydrothermal synthesis of mesoporous magadiite plates via heterogeneous nucleation. *Clays Clay Miner.* **2013**, *61*, 525–531.
- (24) Snæbjörnsdóttir, SÓ; Gislason, S. R.; Galeczka, I. M.; Oelkers, E. H. Reaction path modelling of in-situ mineralisation of CO2 at the CarbFix site at hellisheidi, SW-iceland. *Geochim. Cosmochim. Acta* 2018, 220, 348–366.
- (25) Xiong, W.; Wells, R. K.; Horner, J. A.; Schaef, H. T.; Skemer, P. A.; Giammar, D. E. CO2 mineral sequestration in naturally porous basalt. *Environ. Sci. Technol. Lett.* **2018**, *5*, 142–147.
- (26) Kelemen, P. B.; Matter, J. In situ carbonation of peridotite for CO2 storage. Proc. Natl. Acad. Sci. U. S. A. 2008, 105, 17295–17300.
- (27) Krevor, S. C.; Lackner, K. S. Enhancing serpentine dissolution kinetics for mineral carbon dioxide sequestration. *Int. J. Greenhouse Gas Control* **2011**, *5*, 1073–1080.

- (28) Zhao, H.; Park, Y.; Lee, D. H.; Park, A. A. Tuning the dissolution kinetics of wollastonite via chelating agents for CO 2 sequestration with integrated synthesis of precipitated calcium carbonates. *Phys. Chem. Chem. Phys.* **2013**, *15*, 15185–15192.
- (29) Bourg, İ. C.; Beckingham, L. E.; DePaolo, D. J. The nanoscale basis of CO2 trapping for geologic storage. *Environ. Sci. Technol.* **2015**, 49, 10265–10284.
- (30) Fitts, J. P.; Peters, C. A. Caprock fracture dissolution and CO2 leakage. *Rev. Mineral. Geochem.* **2013**, *77*, 459–479.
- (31) Huang, X.; Chang, J. Synthesis of nanocrystalline wollastonite powders by citrate—nitrate gel combustion method. *Mater. Chem. Phys.* **2009**, *115*, 1–4.
- (32) Speakman, K. The stability of tobermorite in the system CaO-SiO2-H2O at elevated temperatures and pressures. *Mineral. Mag. J. Mineral. Soc.* 1968, 36, 1090–1103.
- (33) Shaw, S.; Clark, S. M.; Henderson, C. Hydrothermal formation of the calcium silicate hydrates, tobermorite (ca 5 si 6 O 16 (OH) 2·4H 2 O) and Xonotlite (ca 6 si 6 O 17 (OH) 2): An in situ synchrotron study. *Chem. Geol.* **2000**, *167*, 129–140.
- (34) Han, F. X.; Banin, A. Selective sequential dissolution techniques for trace metals in arid-zone soils: The carbonate dissolution step. *Commun. Soil Sci. Plant Anal.* **1995**, *26*, 553–576.
- (35) Daval, D.; Martinez, I.; Guigner, J.; Hellmann, R.; Corvisier, J.; Findling, N.; Dominici, C.; Goffe, B.; Guyot, F. Mechanism of wollastonite carbonation deduced from micro-to nanometer length scale observations. *Am. Mineral.* **2009**, *94*, 1707–1726.
- (36) Ashraf, W.; Olek, J. Carbonation behavior of hydraulic and non-hydraulic calcium silicates: Potential of utilizing low-lime calcium silicates in cement-based materials. *J. Mater. Sci.* **2016**, *51*, 6173–6191.
- (37) Given, R. K.; Wilkinson, B. H. Kinetic control of morphology, composition, and mineralogy of abiotic sedimentary carbonates. *J. Sediment. Res.* **1985**, 55, 109–119.
- (38) Cailleteau, C.; Angeli, F.; Devreux, F.; Gin, S.; Jestin, J.; Jollivet, P.; Spalla, O. Insight into silicate-glass corrosion mechanisms. *Nat. Mater.* **2008**, *7*, 978.
- (39) Weissbart, E. J.; Rimstidt, J. D. Wollastonite: Incongruent dissolution and leached layer formation. *Geochim. Cosmochim. Acta* **2000**, *64*, 4007–4016.
- (40) Zakaznova-Herzog, V. P.; Nesbitt, H. W.; Bancroft, G. M.; Tse, J. S. Characterization of leached layers on olivine and pyroxenes using high-resolution XPS and density functional calculations. *Geochim. Cosmochim. Acta* **2008**, *72*, 69–86.
- (41) Wang, F.; Giammar, D. E. Forsterite dissolution in saline water at elevated temperature and high CO2 pressure. *Environ. Sci. Technol.* **2013**, *47*, 168–173.